FINAL RESEARCH REPORT

05/2011 - 10/2012 (18 months)

Dr. Sebastián Costamagna

Instituto de Física de Rosario,
Boulevard 27 de Febrero 210 bis,
2000 Rosario, Argentina

BELSPO Postdoctoral fellowship

(Promotor: Prof. F. Peeters)

Universiteit Antwerpen,
Department of Physics,
Groenenborgerlaan 171,
2020 Antwerpen, Belgium

Abstract

Keywords

Graphene, Graphene nanoribbons, Graphene nanotubes, Electronic properties.

Graphane, Boron-Nitride hexagonal single layer, Thermo-mechanical properties.

The research performed during the realization of the postdoctoral studies were directed to the investigation of electronic and thermo-mechanical properties of graphene and graphene related materials such us graphene nanoribbons, graphene nanotubes, hydrogenated graphene and the boron-nitride hexagonal single layer. The systems considered and the obtained results can be summarized as follows:

(i) The conductance through graphene nanoribbons (GNR) connected to a partially unzipped carbon nanotube (CNT) was studied in the presence of an external magnetic field applied parallel to the long axis of the tube by means of non-equilibrium Green's function technique. We considered CNTs that are partially unzipped to form armchair-GNR/zigzag-CNT/armchair-GNR or zigzag-GNR/ armchair-CNT/zigzag-GNR junctions. We found that the inclusion of a longitudinal magnetic field affects the electronic states only in the CNT region, leading to the suppression of the conductance at low energies. We demonstrated that both types of junctions can be used as magnetic field sensors.

(ii) Thermal fluctuations of a single layer hydrogenated graphene were investigated using large scale atomistic simulations. By analyzing the mean square value of the height fluctuations $<h^2>$ and the height-height correlation function H(q) for different system sizes and temperatures, we showed that hydrogenated graphene is an unrippled system in contrast to graphene. The height fluctuations are bounded, which was confirmed by the behavior of H (q) tending to a constant in the long wavelength limit instead of showing the characteristic scaling law $q^{(4-\eta)}$ (η approx. 0.85) predicted by membrane theory. This unexpected behavior persists up to temperatures of at least 900 K and is a consequence of the fact that in graphane the thermal energy can be accommodated by in-plane bending modes, i.e., modes involving C-C-C bond angles in the buckled carbon layer, instead of leading to significant out-of-plane fluctuations that occur in graphene.

(iii) Using atomistics we investigated the thermodynamical properties of a single atomic layer of hexagonal boron-nitride (h-BN). The thermal excited ripples of large scale single h-BN sheets were calculated and compared to those found for graphene (GE). We found that the h-BN sheet is a less stiff material as compared to graphene. The bending rigidity of h-BN is about 16% smaller than the one of GE at room temperature (300 K), and it increases with temperature as it occurs in GE.

Publication List

1) Partially unzipped carbon nanotubes as magnetic field sensors, S. Costamagna, A. Schulz, L. Covaci, and F. Peeters, Appl. Phys. Lett. **100**, 232104 (2012).

2) Thermal rippling behavior of graphane, S. Costamagna, M. Neek-Amal, J. H. Los, and F. M. Peeters, Phys. Rev. B **86**, 041408(R) (2012).

3) Thermo-mechanical properties of a single hexagonal boron nitride sheet, S. K. Singh, M. Neek-Amal, S. Costamagna, F. M. Peeters, submitted for publication in Phys. Rev. B (July 2012).

4) Thermo-mechanical properties of fluorographene, S. K. Singh, S. G. Srinivasan , M. Neek-Amal, S. Costamagna, Adri C. T. van Duin, and F. M. Peeters, in progress.

5) Melting temperature: From graphene to fluorographene, S. K. Singh, M. Neek-Amal, S. Costamagna, and F. M. Peeters, in progress.

6) Damping of acoustic phonons in graphene, S. Costamagna, K. H. Michel, B. Verberck, and F. M. Peteers, in progress.

Travels for scientific purposes

Visit to discuss scientific results with the Group of Prof. Dr. Annalisa Fasolino (20/09/2011)
Institute for Molecules and Materials, Radboud University, Nijmegen, The Netherlands.

Attendance of meetings / conferences

International School of Solid State Physics - 52nd Course and 53rd Workshop
July 26 - August 7, 2011, Erice, Italy.

Collaborations during postdoc fellowship

(i) CMT Group – Antwerp University

L. Covaci - Postdoc (FWO)

A. Shulz - Postdoc

S. K. Singh - Phd Student

K. H. Michel - Professor Emeritus

B. Verberck - Postdoc (FWO)

F. M. Peteers - Head of the Group

(ii) External collaborators

* M. Neek-Amal,

Department of Physics, Shahid Rajaee Teacher Training University, Lavizan, Tehran 16785-136, Iran .

* J. H. Los,

Institute of Physical Chemistry and Center for Computational Sciences, Johannes Gutenberg University Mainz, Staudinger 9, Mainz, Germany .

* Adri C. T. van Duin,

Department of Mechanical and Nuclear Engineering, Pennsylvania State University, 136 Research East Building, University Park 16802, USA.

Future collaboration

From the next year (2013) Dr. Costamagna will become researcher in the CMT group at the Instituto de Física de Rosario (IFIR-CONICET) in Rosario, Argentina. The research projects currently in progress mentioned above will be continued. A scientific project titled “Theoretical study of thermal conductivity, phonon damping and anharmonic phononic couplings in graphene and graphene multilayers” (promotors: Prof. F. M. Peteers (Flanders) and Dr. Costamagna (Argentina)) has been submitted to the international collaboration program between the Research Foundation of Flanders (FWO) and the Ministry for Science Technology and Productive Innovation of the Argentine Republic (MINCyT) (2013/2014).

I. Partially unzipped carbon nanotubes as magnetic field sensors

Among the existing available techniques to produce GNRs [1,2,3,4], a very appealing one is the unzipping of CNTs. This can be done, for example, by using chemical attack [5] or throught plasma beam etching [6]. Although recent molecular dynamics studies have shown that dangling bonds tend to re-bond on partially unzipped CNT, by fully hydrogenating the opened edges this self-healing behavior can be suppressed [7]. Thus, it is feasible that multi-junctions composed of CNTs and GNRs can be fabricated in the near future. From a theoretical point of view, the electronic transport properties of such junctions have been addressed in a series of works. In Ref. [8] the conductance of partially unzipped aCNT/zGNR junctions was numerically studied. The case of unzipped zCNT was addressed in Refs. [9, 10] where analytical expressions for the wave functions and transmission probabilities were obtained by connecting different parts of the system under proper boundary conditions. The main result is that the metallic aGNR/zCNT/aGNR junctions exhibit perfect transmission for incident low-energy electrons. Different from previous works, here we are interested to study the conductance of partially unzipped CNT in the presence of an external magnetic field parallel to the tube axis. Here, we analyze the aGNR/zCNT/zGNR and zGNR/aCNT/zGNR junctions schematically displayed in Fig. 1 and we show that variations in the external magnetic field can dramatically change the conductance of the system and therefore we propose to use these systems as magnetic field sensors. Such sensors have the additional advantage that much better contacts can be realized on the ribbon sections as compared to plain nanotubes. In order to describe the electron hopping between the π orbitals pertaining to neighboring carbon atoms we adopt a nearest-neighbor tight binding Hamiltonian. The unzipped systems studied here (a) zCNT and (b) aCNT, are displayed in Fig. 1. Note that, for simplicity we have adopted a different enumeration N_x and N_y to define each geometry and that periodic boundary conditions are used at the two edges to define the tubes.

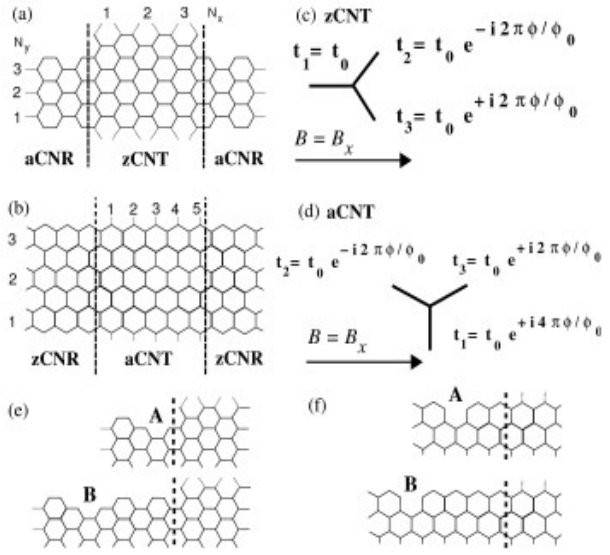

Figure 1: (a) aGNR/zCNT/aGNR and (b) zGNR/aCNT/zGNR junctions. The dashed thick vertical lines separate each part of the system considered for the conductance calculation. The Peierls factors (c-d) modifying the hopping amplitudes in the CNTs appearing due to the magnetic fields are $\phi = B\, r\, a\, \sqrt{(3)}/2$ for the zCNT and $\phi = B\, r\, a/2$ for the zCNT. The size of the zCNT (aCNT) is defined by $N_x=3$ and $N_y=3$ ($N_x= 5$ and $N_y=3$) as indicated on the plot. Edge vacancies considered in this work are displayed in (e) and (f).

When a CNT is partially unzipped we model it as a CNT that is connected to ribbons on both of its sides. The aGNR/zCNT/aGNR system can be thought of as a zCNT from which one line of C-atom dimers is removed in the left and right section, forming the aGNR-leads. In the zGNR/aCNT/zGNR system, no atoms are removed, but the bonds between two zigzag edges are removed. In both cases the model Hamiltonian describing the whole system is therefore given by

$$H = H_{z(a)CNT} + H_{a(z)GNR_L} + H_{a(z)GNR_R} \qquad (1)$$

where $H_{a(z)GNR\{L(R)}$ corresponds to the semi-infinite left (right) lead, and $H_{z(a)CNT}$ describes the nanotube. In addition to these terms we have h_{LC} and h_{LR} which are the hopping amplitudes connecting the leads to the nanotube. The hopping parameter between carbon atoms, t_0=2.7 eV, is taken as unit of energy. The conductance calculation was done by using the non equilibrium Green's function technique [11,12,13] where G(E) is obtained from the transmission function T(E) as $G(E)=(2e^2/h)\ T(E)$. We remark that the self-energies for the semi-infinite leads have been computed self-consistently and when used to calculate the G(E) of pure CNTs and GNRs they give the expected value as shown in Fig. 2.

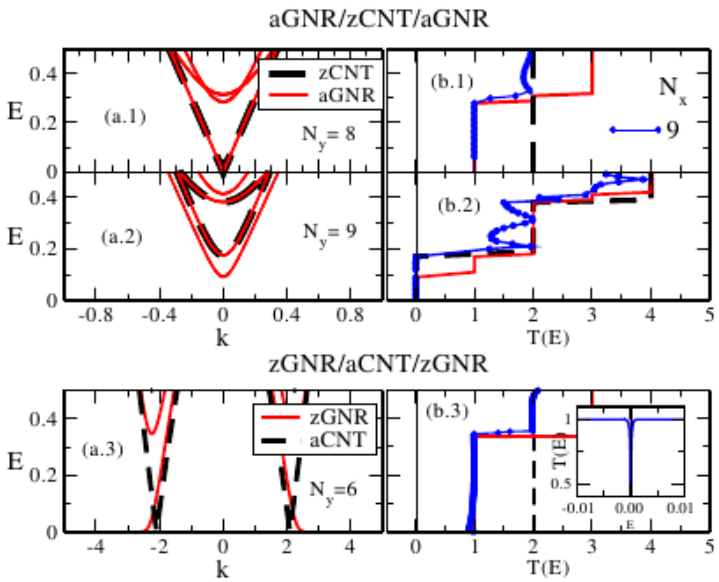

Figure 2: (a) Bandstructure of pure CNTs (dashed lines) and GNRs (solid lines) as indicated. T(E) for each corresponding junction is shown in (b) for N_x=9. T(E) for the pure CNTs (dashed lines) and GNR (solid lines) were included for a better comprehension. The inset shows the vanishing of T(E) at very low energies in the case of zGNR/aCNT/zGNR junctions.

Even without external magnetic field, very different low energy electronic properties can be present in these junctions. In the case of zCNTs/aGNRs, it is known that the metallicity of undoped samples is determined by the width of the tubes and ribbons [9]. In Fig. 2, panels (a.1) and (a.2) show the low energy band-structure for pure infinitely long aGNRs and zCNTs of different widths. In both, the metallic and the semiconducting regimes, only some of the bands of the aGNR coincide with the bands of the zCNT due to the different transverse boundary condictions (open vs. periodic), see e.g. Ref. [9]. For the partially unzipped aGNR/zCNT/aGNR metallic junctions, i.e. N_y=8, it is expected that in the absence of the magnetic field the system should show no backscattering and a perfect conductance at low energies [9]. Accordingly we see in Fig. 2 (b.1) that the transmission remains unity at low energies. For higher energies G(E) shows the expected jumps each time that a new channel is available for conduction.

On the other hand, in the case of the zGNR/aCNT/zGNR junction (Fig.2 (a.3) and (b.3)) we observe a quite different low energy behavior. While zGNRs are always metallic independent of their width, due to the localized edge states at zero energy, T(E) vanishes in the combined system when the energy approaches zero, which is made more clear in the inset of Fig. 2. This sharp drop in the conductance at zero energy can be understood from the mismatch in the dispersion of the zGNR and aCNT subsystems, (cf. Fig. 2 (a.3)), as the energy approaches zero. Due to the resulting difference in momentum of the corresponding eigenstates, electron wave-functions incident from the ribbon become evanescent in the aCNT and therefore the conduction is suppressed. Although not shown here, we have found that this suppression is sensitive to the length of the aCNT subsystem, as the electron tunnels through it.

When an external magnetic field is acting on the CNTs it can be included into the tight binding Hamiltonian using the so-called Peierls phase. For a magnetic field parallel to the tube axis, this is $B=B_x$, there will be only three different hopping phases. These terms were displayed in Fig. 1(c) and Fig. 1(d). $\phi_0=h/e$ is the quantum flux, r is the radius of the tube, B is the magnitude of the magnetic field and a=1.42 Å is the carbon atoms distance. For the GNR the axial magnetic field has no effect since the flux through the ribbon is zero.

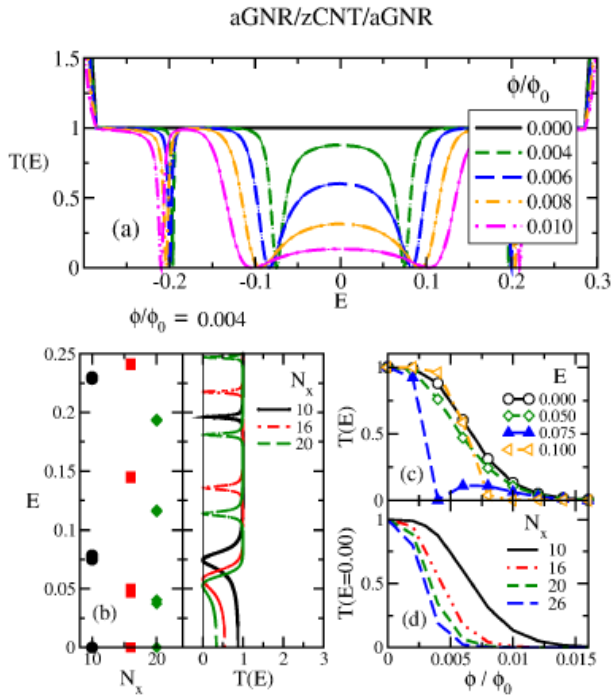

Figure 3: (a) T(E) in the unzipped zCNT (N_y=8, N_x=10) for different magnetic fields. (b) Low energy spectrum of an isolated zCNT and T(E) for different tube lengths. ϕ/ϕ_0 =0.004 and N_y=8 in both cases. (c) Variation of T(E) for several energies near zero (extracted from (a)) and (d) decay of T(E=0.00), for several tube length as indicated, against the magnetic field.

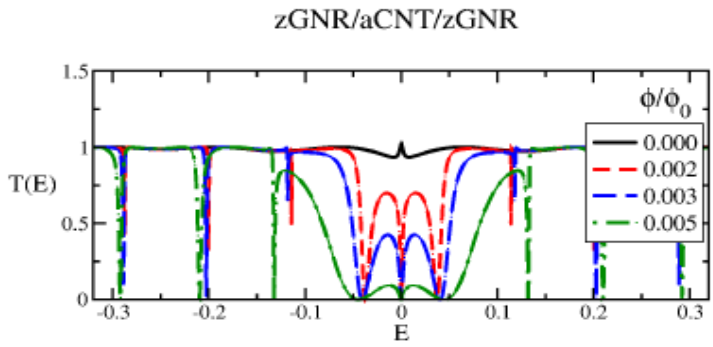

Figure 4: Variation of T(E) in the unzipped aCNT (N_y=6, N_x=24) for different magnetic fields as indicated on the plot.

The effect of the magnetic field on the aGNR/zCNT/aGNR junction is shown in Fig. 3. At low energies the transmittance is suppressed due to the magnetic field induced gap in the zCNT (this comes about because the magnetic field will shift the transverse momentum thus changing a metallic nanotube into a semiconducting one). The suppression is due to a decrease of the overlap of evanescent modes from the aGNR and depends on the tube length as can be seen in Fig. 3(b). Thus, when the transmittance vs. magnetic flux is plotted for different energies and tube lengths, as shown in Figs. 3(c-d), we notice that this junction could be used as a magnetic sensor since the resistance of the junction is very sensitive to magnetic field changes. The longer the tube length, the more sensitive the sensor will be since smaller magnetic fields are needed to suppress the overlap of the wave functions coming from the leads. When the Fermi level is shifted from the Dirac point for certain energies, which depends on the tube length, the transmittance is even more sensitive to changes in the magnetic field thus improving the efficiency of the sensor. For the zGNR/aCNT/zGNR junction, the dependence of the transmittance is presented in Fig. 4. Except to the peculiar zero energy suppresion, the behavior is similar to the aGNR/ZCNT/aGNR junction thus making the operation of the proposed magnetic sensor independent of the orientation of the partially unzipped CNTs.

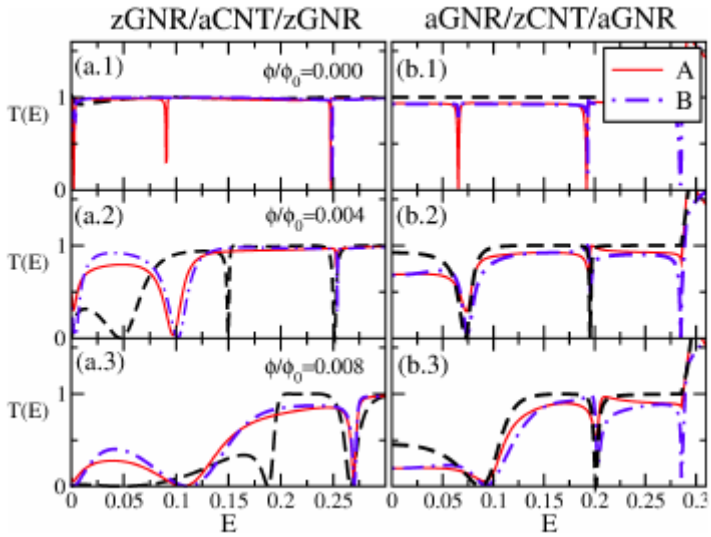

Figure 5: Effect of edge vacancies on T(E) in the (a) zGNR/aCNT/zGNR (N_x=10, N_y=6) and (b) aGNR/ZCNT/aGNR (N_x=10, N_y=8) junctions for different magnetic fields as indicated. The location of the vacancies named A and B is displayed in Figs. 1(e,f). T(E) for the case where there are no vacancies indicated by the black-dashed line.

The performance of these magnetic field sensors could be affected by defects. The effect of defects as Carbon atom vacancies on the edges of the ribbons, where they are more likely to appear in the unzipping process, is shown in Fig. 5. While edge defects modify the conductance, their effects can be clearly distinguished from the effects of the magnetic field thus even in the presence of defects the partially unzipped CNT are still feasible as magnetic field sensors.

To conclude: Magnetic field induced changes of the electronic properties in the zCNT/aGNR regions will modify the magneto-resistance of the junctions which hence can be used as magnetic field sensors. While more realistic system sizes are out of the scope of the numerical technique employed, given a tube radius of r=500 nm, ϕ/ϕ_0 equals to 0.001 which implies a magnetic field B of approx. 0.67-1.16 T depending on the junction. Therefore, the simplicity of the sensor, due to the fact that the GNRs are perfect contacts to the CNTs while the magnetic field does not affect the contacts, makes it interesting for possible applications. Edge defects in the ribbons do not modify the qualitative behavior of the junctions and their effect on the conduction can be neglected when the defects are far from the junction (e.g. farther than 1nm). Also, due to the extraordinary stiffness of CNTs, in the relaxed configuration the nanotube region is expected to be straight and therefore curvature effects can be safely neglected.

II. **Thermal excited ripples in hydrogenated graphene (Graphane)**

Hydrogenated graphene (GE), called graphane (GA), is a quasi-two-dimensional (2D) structure of carbon (C) atoms ordered in a buckled honeycomb lattice covalently bonded to hydrogen (H) atoms in an alternating, chairlike arrangement [14]. Experimentally, it has been shown that GA can be obtained reversibly starting from a pure GE layer [15], and since then it has become a material of high interest due to its potential applications in nanoelectronics [16]. As compared to GE, the chemisorption of the H atoms is accompanied by an important reconstruction of the chemical bonds and angles in the flat honeycomb lattice [17]. Each carbon atom acquires an H neighbor, involving a transition from sp^2 to sp^3 hybridization, which turns the conjugated, graphitic C-C bonds into single C-C bonds, changing locally the planar shape of graphene into an Åtrom scale out-of-plane buckled shaped membrane [18], as displayed schematically in Fig. 6.

One expects that at nonzero temperature thermally excited ripples will occur and distort the lattice. For GE these ripples can be described theoretically by elasticity theory of continuum membranes [19]. Among others, this membrane theory predicts a suppression of the long wavelength out-of-plane fluctuations by the anharmonic coupling between the out-of-plane bending and in-plane stretching modes, leading to a characteristic power law behavior for the height fluctuations as a function of the system size. Although the height fluctuations still diverge, the normal-to-normal correlation is preserved over a large length scale, stabilizing the membrane. By using atomistic simulations these results were shown to be applicable to GE, implying that this prototype 2D solid behaves as a membrane [20, 21], and also to bilayer GE [22]. Experiments have confirmed that suspended GE is not perfectly flat but instead presents ripples at finite temperatures [23].

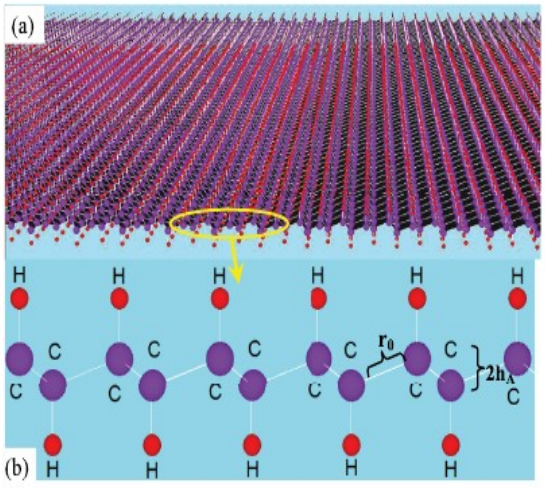

Figure 6: (a) Schematic view of a large sample of graphane. (b) Buckling between C atoms in the A (higher) and B (lower) sublattices at T = 300 K.

Here, we study thermally excited ripples in GA using state-of-the-art molecular dynamics (MD) simulations and show that the Åtrom scale thermal ripples present in GE do not appear in GA for temperatures up to at least 900 K. The A- and B-sublattice buckling is preserved and inhibits the formation of long wavelength ripples. As a consequence, the calculated height-height correlation function H (q) does not follow the characteristic $q^{(4-\eta)}$ power law scaling in the long wavelength limit predicted by membrane theory, and the height fluctuations appear to be bounded. According to membrane theory and within the harmonic approximation, applicable in the short wavelength regime where q is larger than some crossover value q^*, the out-of-plane and in-plane modes are decoupled and the elastic bending free energy density is described by $F_{harm} = \kappa(\nabla^2 h)^2$, where h is the local height and κ is the bending rigidity of the membrane which governs the properties of the temperature induced ripples. Substitution of the Fourier transform of h and integrating over 2D space leads to the following height-height correlation function,

$$H_{\text{harm}}(q) = \langle |h(q)|^2 \rangle = \frac{N k_B T}{\kappa S_0 q^4}, \qquad (2)$$

where N is the number of atoms, S_0 the surface area per atom, and k_B is the Boltzmann constant. Accordingly, the height fluctuations in the harmonic regime behave as $\langle h^2 \rangle_{harm} = CL^2$, with C a temperature-dependent constant and L the linear size of the system. In the large wavelength limit, i.e., for $q < q^*$, the height fluctuations are suppressed by the mentioned anharmonic coupling between bending and stretching modes giving rise to a renormalized q-dependent bending rigidity $\kappa \propto q^{(-\eta)}$ and a power law scaling behavior

$$H(q) = \frac{N k_B T}{\kappa S_0 q^{4-\eta}},$$

and accordingly $h^2 = C\, L^{(2-\eta)}$ with C a constant (=C). The universal scaling exponent η has been estimated to be 0.821 [24]. For GE, using Monte Carlo (MC) simulations with the empirical long-range carbon bond-order potential II (LCBOPII), good agreement with these results, derived from continuum theory, was found with $\eta \approx 0.85$. Here, we investigate to which extent membrane theory

can be applied to the description of thermally excited ripples in GA and we compare our results with those for GE. To calculate the height fluctuations for GA we first need to define an appropriate value for the height h_i of each lattice site i. Since we are mainly interested in the long wavelength fluctuations, which normally govern the size of the height fluctuations, we defined it on the basis of the carbon positions as

$$h_i = \frac{1}{2}\left(z_i + \frac{1}{3}\sum{}'_j z_j\right),$$

where i is a carbon atom, j runs over the three carbon neighbors of i, and z_i is the z coordinate perpendicular to the plane. This definition allows for a straightforward comparison with GE, for which the heights were defined in the same way following previous work [20]. To measure h^2 and H (q) we have performed MD simulations using the LAMMPS package. Both the GA and the GE systems have been sampled using the constant NPT ensemble (with P = 0). For the interatomic interactions we used the modified second generation of Brenner's bond-order potential, i.e., adaptive intermolecular reactive bond-order (AIREBO), which has been shown to predict correctly the configurations for many different hydrocarbon structures. We simulated square shaped systems with the number of C atoms equal to N = 4860, 8640, 19 440, and 37888, in a temperature range from 100 to 900 K (note that for GA the total number of atoms is twice as large). Periodic boundary conditions were applied in the x and y directions.

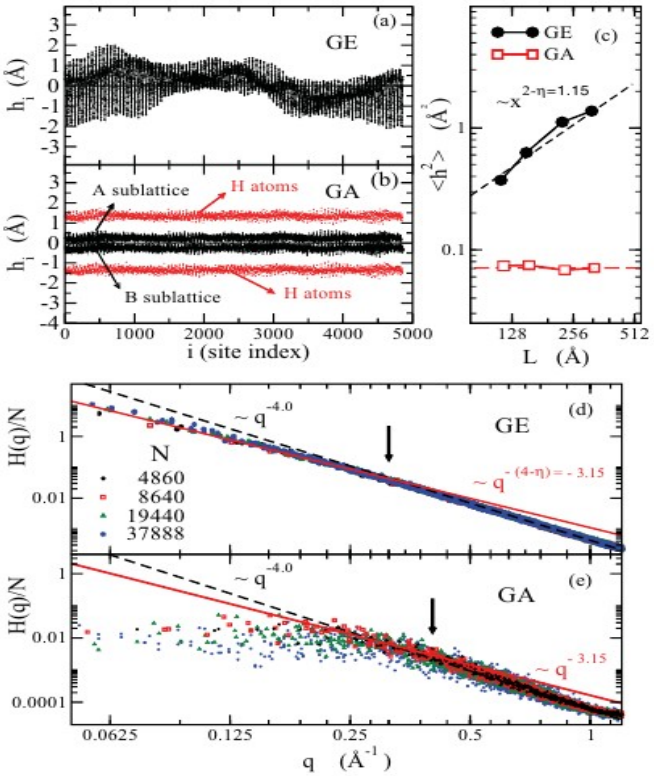

Figure 7: Heights of the C atoms in the GE (a) and GA (b) against the site index for arbitrary snapshots taken during the MD simulation. N = 4860. T = 300 K. (c) h^2 against $L = L_x * L_y$ in GE (circles) and GA (squares). H (q) for different system sizes as indicated for (d) GE and (e) GA. The dashed line shows the harmonic q^{-4} behavior and the solid line the correction due to anharmonic coupling for small q. Vertical arrows roughly indicate q^* below which the harmonic behavior is broken.

The results have been computed averaging over 300–500 uncorrelated configurations. In Fig. 7 we show the out-of-plane positions for GE (a) and GA (b) for arbitrary snapshots taken during the simulation at room temperature. In GA, the A and B sublattices fluctuate around their mean heights $h_{A,B} \sim \pm 0.256$ Å. The scaling of h^2 with the system size is displayed in Fig. 7(c). The obtained values for GE are in close agreement with previous reported MD results obtained with the reactive empirical bond-order (REBO) potential and slightly lower than those obtained from MC simulations using the LCBOPII [25]. For GE, h^2 increases as $L^{(2-\eta)}$ as expected from membrane theory. For GA, instead, h^2 is almost independent of the system size. The differences in the rippling behavior of GA and GE are also evident from the results for H(q) [Figs. 7(d) and 7(e)]. As it should be, the H(q) functions for different system sizes overlap. However, for GA, although the harmonic q^{-4} behavior for short wavelengths is well recovered, H(q) tends to a constant in the long wavelength limit. Hence, it does not follow the $q^{4-\eta}$ power law as expected from membrane theory and found for GE.

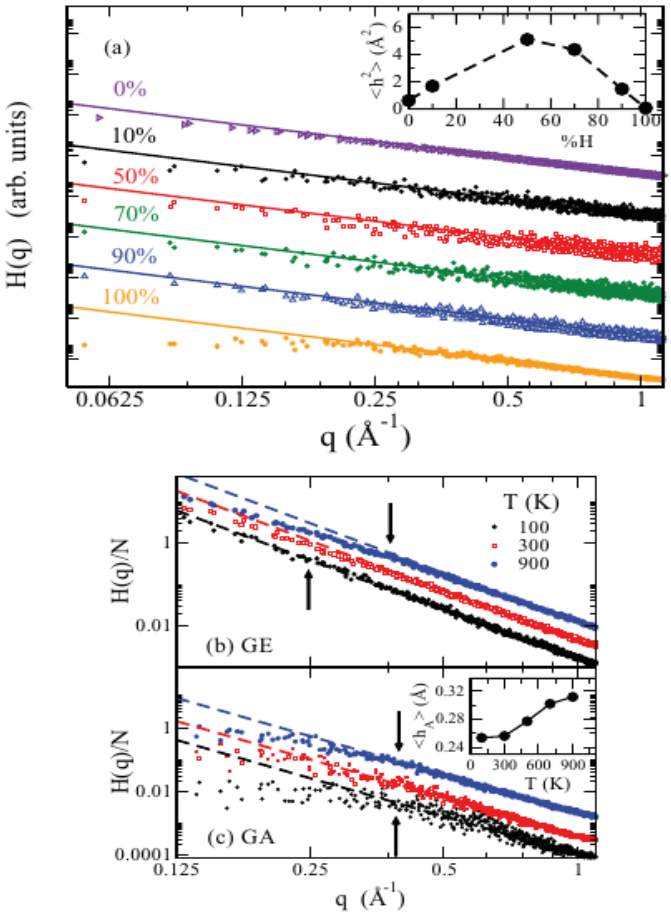

Figure 8: (a) H (q) at 300 K for different % of H atoms (0% correspond to GE and 100% to GA). The different curves have been shifted for a better comparison. In the inset we show the variation of h^2. H (q) for different temperatures as indicated for (b) GE and (c) GA. The inset of (c) shows the average value of the heights in the A sublattice of C atoms against temperature. N = 8640.

The intermediate regimes where GE is only partially covered by H atoms are analyzed in Fig. 3(a). Notice that H(q) displays harmonic behavior even for a H coverage as large as 90%. The deviations at low wave vectors are small and hence can be ascribed to anharmonic coupling. The variation of h^2, shown in the inset, indicates that first the sheet is softened when partially hydrogenated and becomes stiff at full coverage. The behavior of H(q) for different temperatures is

shown in Figs. 8(b) and 8(c). As expected, with increasing temperature H(q) is shifted to larger values for both GE and GA. In the inset of Fig. 8(c) we show the average heights of the C atoms in the A sublattice against temperature. We also found that $h_A \sim - h_B$ over the whole temperature range, implying that the A- and B-sublattice buckling is preserved.

More signals of the differences between the corrugations in GA and GE comes from the temperature dependence of h^2 shown in Fig. 4(a). Note the difference in the vertical scale displayed on the left- and right-hand sides for GE and GA, respectively. While for GE the value of h^2 changes about 0.61 Å between 100 and 900 K, the variation is only 0.07 Å for GA, indicating that GA remains approximately un-rippled even at 900 K. The variation of q^* against T [Fig. 9(b)] also shows the same almost constant behavior for GA, whereas for GE, $q^*(T)$ behaves as expected for a 2D membrane [20]. From the calculated $H(q \rightarrow \infty)$ at different T and Eq. (2), one can also determine the T dependence of the bending rigidity κ. Using the REBO potential it was found that κ decreases with T for GE, similarly as for liquid membranes. However, the opposite behavior was found using the LCBOPII potential [20]. In Ref. [26] the rigidity was found to depend on the system size. Thus, the reported values for κ in GE vary from 0.79 to 2.13 eV depending on the calculation method [27]. In Fig. 9(c) we show κ for GE and GA calculated from the harmonic part of H(q) between q = 0.5 and 1 $Å^{-1}$, confirming that for GE, κ increased with T. For GA, κ is much larger and, most surprisingly, κ strongly decays when temperature is increased, opposite to the behavior for GE. The reason why GA does not obey membrane theory should be found in the geometry of the buckled carbon layer which allows for low energy in-plane bending modes, involving the C-C-C angles. These accordion types of modes have a relatively low energy. In principle this comes down to a strong anharmonic coupling of the out-of-plane bending mode with these in-plane bending accordion modes which strongly damp the out-of-plane excitations.

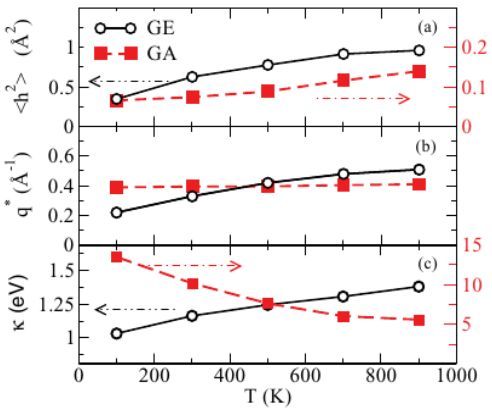

Figure 9: Variation of (a) h^2 , (b) q and (c) κ against temperature for GE (circles) and GA (squares). N = 8640.

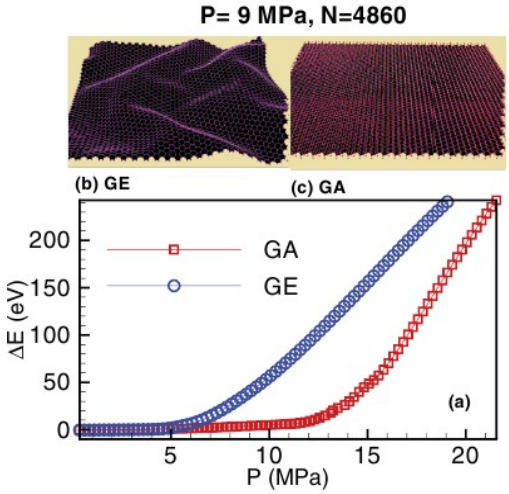

Figure 10: (a)Energy increase under biaxial pressure with respect to the relaxed system at zero pressure for GA and GE (0 K). Shape of (b) GE and (c) GA for P = 9 MPa. Note that while GE is corrugated, GA instead remains unrippled.

To illustrate this further we have performed NPT simulations for increasing pressure, the results of which are shown in Fig. 10. It shows that GA resists much higher pressures before bending than GE. Using MD simulations we have shown that the intrinsic thermal ripples present in GE do not appear in GA for temperatures up to at least 900 K, which we ascribe to the Åtrom scale buckling of the carbon layer in GA into a carbon bilayerlike configuration. The rippling behavior of GA is in disagreement with the continuum elasticity theory of membranes. The results from membrane theory are supposed to be universal, which means that they should not depend on the atomic scale details within the membrane. Instead, we find that GA can accommodate the thermal energy by in-plane bending modes, i.e., modes involving C-C-C bond angles in the buckled carbon layer instead of leading to significant out-of-plane fluctuations that occur in graphene. The present results for GA suggest that membranes of atomic scale thickness can exhibit a more complicated behavior than predicted by membrane theory.

III. **Thermomechanical properties of a single hexagonal boron nitride sheet**

The single layer of hexagonal boron-nitride (h-BN) is a wide gap insulator that is very promising for opto-electronic technologies [28, 29], tunnel devices and field-effect transistors [31, 30, 31]. h-BN ribbons doped by carbon has been proposed [32, 33]. In addition, BN based nanostructures are potential materials for thermal management applications [34–40]. Therefore, the knowledge of the shape and the temperature dependence of the intrinsic ripples is fundamental for novel nano-devices based on this material.

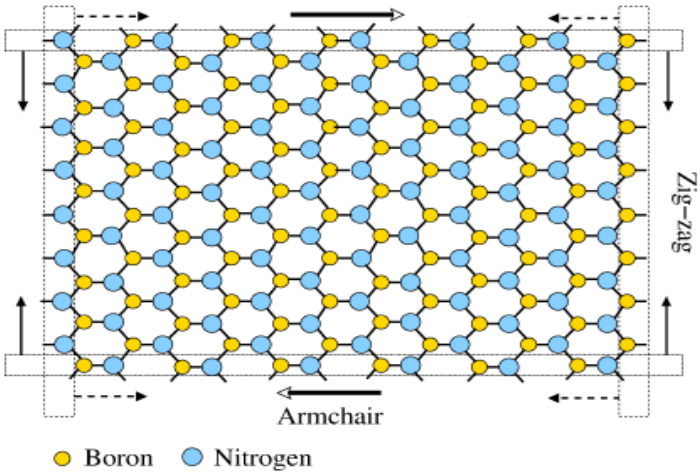

Figure 11: Schematic view of the single h-BN sheet. Smaller-yellow (bigger-blue) circles refers to the B (N) atoms. The rectangles indicate the atoms that are fixed during compression. Dashed (straight) lines correspond to zig-zag (armchair) uniaxial compression in the direction given by the arrows. Open arrows indicate the shear stress applied in the armchair direction.

Both GE and h-BN sheets have a honeycomb lattice structure, however the different electronic properties and phonon band structure [41–43] results in unequal morphologies and corrugations. First-principle calculations have been performed using small unit cells, periodically replicated, which are unable to model long wavelenght corrugations which require thousands of atoms. Conversely, atomistic simulations using molecular dynamics simulations (MD) enable to study thermo-mechanical properties directly on large scale samples. The modified Tersoff potential [44] (TP) (parameterized originally for carbon and silicone) with various set of parameters have shown to predict reasonable values for the thermo-mechanical properties of the h-BN sheet. In the

pioneering work by Albe *et al*. reparameterized TP was used to study the impact of energetic boron and nitrogen atoms on a cubic-BN target [45]. Some other groups have also parameterized TP using various experimental data, e.g. Sekkal et al. [46] treated h- N as a one-component system, using the same potential parameters for both boron (B) and nitrogen (N) (neglecting the B-N interaction) to investigate the structural properties. Matsunaga *et al*. [47] proposed the TP of B in order to simulate cubic boron carbonitrides which are compatible with the parameters of nitrogen fitted by Kroll [48], and recently, Liao *et al*. [49] and Sevik *et al*. [50] reported TP parameters that were used to study the mechanical properties and the thermal conductivity of a h-BN sheet, respectively.

In this study, we investigate the thermal rippling behavior of free standing monolayer h-BN by using state of the art molecular dynamics (MD) simulations. We adopted the TP potential reparametrized by Sevik et al. which has been shown to obtain the experimental structure and the phonon dispersion of the two-dimensional h-BN sheet. As we describe below we found that h-BN is more corrugated and a less stiff material as compared to GE.

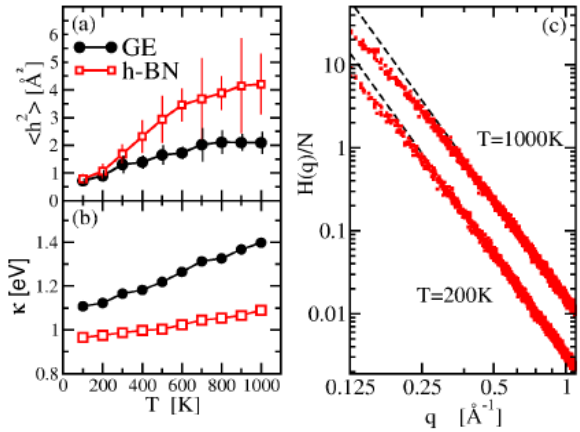

Figure 12: Variation of (a) $< h^2 >$ and (b) the bending rigidity versus temperature for both h-BN (open squares) and GE (solid circles). (c) Height-height correlation function H(q) of h-BN at two different temperatures as is indicated. The dashed lines indicate the harmonic q^{-4} law.

The out-of-plane fluctuations shown in Fig. 12(a) indicate that in h-BN the increase of temperature creates larger corrugations in h-BN than in GE. The bending rigidity κ, calculated from the harmonic part of H(q) between q=0.5 $Å^{-1}$ and q=1 $Å^{-1}$ and in agreement with the larger values of $<h^2>$, is smaller in h-BN than in GE. Note thatκ for both h-BN and GE increase with temperature. In Fig. 12(c) we show H(q) at 200K and 1000K where the harmonic behavior can be clearly observed (fitted with a dashed line) and, as expected, with increasing temperature H(q) acquire a larger magnitude. This figure also reveals that the ripples are not characterized by an unique wave-length and instead follows the behavior expected from continuum membrane theory. Thus, we found that the h-BN sheet is a less stiff material as compared to graphene. The bending rigidity of h-BN is about 16% smaller than the one of GE at room temperature (300 K), and it increases with temperature as it occurs in GE.

References

[1] H. C. Schniepp, Je-Luen Li, M. J. McAllister, H. Sai, M. Herrera-Alonso, D. H. Adamson, R. K.Prud'homme, R. Car, D. A. Saville and I. A. Aksay, J. Phys. Chem. B **110**, 8535 (2006).

[2] X. Li, X. Wang, Li Zhang, S. Lee and H. Dai, Science **319**, 1229 (2008).

[3] X. Yang, Xi Dou, A. Rouhanipour, L. Zhi, H. J. Rder, and K. Mllen, J. Am. Chem. Soc. **130**, 4216 (2008).

[4] J. Cai, P. Ruffieux, R. Jaafar, Blankenburg, M. Muoth, A. P. Seitsonen, M. Saleh, X. Feng, K. Mllen and R. Fasel, Nature (London) **466**, 470473 (2010).

[5] D. V. Kosynkin, A. L. Higginbotham, A. Sinitskii, J. R. Lomeda, A. Dimiev, B. K. Price, J. M. Tour, Nature (London) **458**, 872 (2009).

[6] L. Jiao, L. Zhang, X. Wang, G. Diankov, H.J. Dai, Nature (London) **458**, 877 (2009).

[7] C. Tang, W. Guo and C. Chen, Phys. Rev. B **83**, 075410 (2011).

[8] H. Santos, L. Chico, and L. Brey, Phys. Rev. Lett. **103**, 086801 (2009).

[9] Y. Klymenko and O. Shevtsov, Eur. Phys. J. B **72**, 2 (2009) 203-209.

[10] Yu. O. Klymenko, Eur. Phys. J. B **77**, 433-440 (2010) .

[11] S. Datta, Electronic Transport in Mesoscopic Systems (Cambridge University Press, Cambridge, U.K., 1995)

[12] H. Xu, T. Heinzel, M. Evaldsson and I. V. Zozoulenko, Phys. Rev. B **77**, 245401 (2008).

[13] S. Costamagna, O. Hernandez and A. Dobry, Phys. Rev. B **81**, 115421 (2010).

[14] M. H. F. Sluiter and Y. Kawazoe, Phys. Rev. B **68**, 085410 (2003); J. O. Sofo, A. S. Chaudhari, and G. D. Barber, ibid. **75**, 153401 (2007).

[15] D. C. Elias, R. R. Nair, T. M. G. Mohiuddin, S. V. Morozov, P. Blake, M. P. Halsall, A. C. Ferrari, D. W. Boukhvalov, M. I. Katsnelson, A. K. Geim, and K. S. Novoselov, Science **323**, 610 (2009).

[16] M. Z. S. Flores, P. A. S. Autreto, S. B. Legoas and D. S. Galvao, Nanotechnology **20**, 465704 (2009); O. Leenaerts, H. Peelaers, A. D. Hernandez-Nieves, B. Partoens, and F. M. Peeters, Phys. Rev. B **82**, 195436 (2010); A. D. Hernandez-Nieves, B. Partoens, and a F. M. Peeters, ibid. **82**, 165412 (2010); H. Sahin, C. Ataca, and S. Ciraci, ibid. **81**, 205417 (2010); X. D. Wen, L. Hand, V. Labet, T. Yang, R. Hoffmann, N. W. Ashcroft, A. Oganov, and A. Lyakhov, Proc. Natl. Acad. Sci. USA **108**, 6833 (2011).

[17] M. Neek-Amal and F. M. Peeters, Phys. Rev. B **83**, 235437 (2011).

[18] D. W. Boukhvalov, M. I. Katsnelson, and A. I. Lichtenstein, Phys. Rev. B **77**, 035427 (2008).

[19] D. Nelson, T. Piran, and S. Weinberg, Statistical Mechanics of Membranes and Surface (World Scientific, Singapore, 2004).

[20] J. H. Los, M. I. Katsnelson, O. V. Yazyev, K. V. Zakharchenko, and A. Fasolino, Phys. Rev. B **80**, 121405 (2009).

[21] R. Roldan, A. Fasolino, K. V. Zakharchenko, and M. I.Katsnelson, ibid. **83**, 174104 (2011); M. Neek-Amal and F. M. Peeters, ibid. **82**, 085432 (2010); Appl. Phys. Lett. **97**, 153118 (2010).

[22] K. V. Zakharchenko, J. H. Los, M. I. Katsnelson, and A. Fasolino, Phys. Rev. B **81**, 235439 (2010).

[23] D. A. Kirilenko, A. T. Dideykin, and G. Van Tendeloo, Phys. Rev. B **84**, 235417 (2011).

[24] P. Le Doussal and L. Radzihovsky, Phys. Rev. Lett. **69,** 1209 (1992).

[25] J. H. Los, L. M. Ghiringhelli, E. J. Meijer, and A. Fasolino, Phys. Rev. B **72**, 214102 (2005).

[26] P. Liu and Y. W. Zhang, Appl. Phys. Lett. **94**, 231912 (2009).

[27] L. J. Karssemeijer and A. Fasolino, Surf. Sci. **605**, 1611 (2011); K. H. Michel and B. Verberck, Phys. Rev. B **78**, 085424 (2008); A. Lajevardipour, M. Neek-Amal, and F. M. Peeters, J. Phys.: Condens. Matter **24**, 175303 (2012).

[28] X. Blase, A. Rubio, S. G. Louie, and M. L. Cohen, Phys. Rev. B **51**, 6868 (1995).

[29] K. Watanabe, T. Taniguchi, and H. Kanda, Nat. Mater. **3**, 404 (2004).

[30] L. Britnell, R. V. Gorbachev, R. Jalil, B. D. Belle, F. Schedin, M. I. Katsnelson, L. Eaves, S. V. Morozov, A. S. Mayorov, N. M. R. Peres, A. H. Castro Neto, J. Leist, A. K. Geim, L. A. Ponomarenko, and K. S. Novoselov, Nano Lett. **12**, 1707 (2012).

[31] G-H. Lee, Y-J. Yu, C. Lee, C. Dean, K. L. Shepard, P. Kim, and J. Hone, Appl. Phys. Lett. **99**, 243114 (2011).

[32] J. Jung, Z. Qiao, Q. Niu, and A. H. MacDonald, Nano Letters (April 2012).

[33] J. Beheshtian, A. Sadeghi, M. Neek-Amal, K. Michel, and F. M. Peeters. Phys Rev. **B** (2012).

[34] N. D. Mermin, and H. Wagner, Phys. Rev. Lett. **17**, 1133 (1966).

[35] J. C. Meyer, A. Geim, M. I. Katsnelson, K. S. Novoselov, T. J. Booth, and S. Roth, Nature (London) **446**, 60 (2007).

[36] A. Fasolino, J. H. Los, and M. I. Katsnelson, Nat. Mater. **6,** 85 (2007).

[37] M. I. Katnelson, and A. K. Geim, Phil. Trans. R. Soc. A **366**, 195 (2008).

[38] T. Ouyang, Y. Chen, Y. Xie, K. Yang, Z. Bao, and J. Zhong, Nanotechnology **21**, 245701 (2010).

[39] I.Savic, D. A. Stewart, and N. Mingo, Phys. Rev. B **78**, 235434 (2008).

[40] D. A. Stewart, I.Savic, and N. Mingo, Nano Lett. **9**, 81 (2009).

[41] C. W. Chang, A. M. Fennimore, A. Afanasiev, D. Okawa, T. Ikuno, H. Garcia, D. Li, A. Majumdar, and A. Zettl, Phys. Rev. Lett. 97, 085901 (2006). H. Shen, Comp. Mater. Sci. **47**, 220 (2009).

[42] Y. Xiao, X. H. Yan, J. X. Cao, J. W. Ding, Y. L. Mao, and J. Xiang, Phys. Rev. B **69**, 205415 (2004).

[43] M. Sakurai, Y. Sakai, and S. Saito, J. Phys.: Conf. Ser. **302**, 012018 (2011). M. Topsakal, E. Akt¨ rk, and S. Ciraci, Phys. Rev. B **79**, 115442 (2009). D. Golberg, Y. Bando, Y. Huang, T. Terao, M. Mitome, C. Tang, and C. Zhi, ACS Nano **4**, 2979 (2010). H. Sahin, S. Cahangirov, M. Topsakal, E. Bekaroglu, E.Akturk, R. T. Senger, and S. Ciraci, Phys. Rev. B **80**, 155453 (2009).

[44] J. Tersoff, Phys. Rev. B **37**, 6991 (1988).

[45] K. Albe and W. Muller, Comput. Mater. Sci. **10**, 111 (1998).

[46] W. Sekkal, B. Bouhafs, H. Aourag, and M. Cartier, J. Phys.: Condens. Matter **10**, 4975 (1998).

[47] K. Matsunaga, C. Fisher, and H. Matsubara, Japan J. Appl. Phys. **39**, 48 (2000).

[48] P. M. Kroll, PhD Thesis (Technische Hochschule Darmstadt, 1996).

[49] M. L. Liao, Y. C. Wang, S. P. Ju, T. W. Lien, and L. F. Huang, J. Appl. Phys. **110**, 054310 (2011).

[50] C. Sevik, A. Kinaci, J. B. Haskins, and T. Cahin, Phys. Rev. B **84**, 085409 (2011).